PHYSICS

Entanglement classifier in chemical reactions

Junxu Li and Sabre Kais*

The Einstein, Podolsky, and Rosen (EPR) entanglement, which features the essential difference between classical and quantum physics, has received wide theoretical and experimental attentions. Recently, the desire to understand and create quantum entanglement between particles such as spins, photons, atoms, and molecules is fueled by the development of quantum teleportation, quantum communication, quantum cryptography, and quantum computation. Although most of the work has focused on showing that entanglement violates the famous Bell's inequality and its generalization for discrete measurements, few recent attempts focus on continuous measurement results. Here, we have developed a general practical inequality to test entanglement for continuous measurement results, particularly scattering of chemical reactions. After we explain how to implement this inequality to classify entanglement in scattering experiments, we propose a specific chemical reaction to test the violation of this inequality. The method is general and could be used to classify entanglement for continuous measurement results.

INTRODUCTION

Entanglement, which is a quantum mechanical property that describes a correlation between quantum mechanical systems that has no classical analog, was introduced by Shrödinger in 1935 (*1*). This phenomenon was the subject of the famous paper by Einstein, Podolsky, and Rosen, known as the EPR paradox (*2*), where they considered such behavior to be impossible and argued that the accepted formulation of quantum mechanics must therefore be incomplete. The debate lasted for nearly 30 years until the proposal of Bell's inequality, which is violated by entanglement (*3*). Entanglement effect was verified experimentally (*4*) in tests where the polarization of photons and spins of entangled particles were measured to be statistically violating Bell's inequality. Nowadays entanglement has become an extremely important physical resource for many applications in quantum communication (*5*–*8*) and quantum computation (*9*–*15*).

Two-particle entanglement has long been demonstrated experimentally, and recently, there are notable achievements to generate entanglement between three and more spatially separated particle systems. For instance, a 10-photon entanglement system was successfully generated experimentally in 2016 (*16*, *17*). There are also observations of entanglement in quantum dots (*18*), nitrogen-vacancy center (NV) in diamond (*19*), trapped ions (*20*), and even entanglement between photon and quantum dots (*21*).

It is very important in all of these experiments to be able to quantify or measure the entanglement. Several methods have been proposed to address this question such as entanglement witnesses (*22*), entropic inequalities (*23*), and quantum state classifier based on machine learning (*24*). However, most of these methods are designed for discrete measurement results. Although there are a few successful theoretical analyses for continuous measurement results, they have focused mainly on photonic systems (*25*–*27*). The most widely used method to classify entanglement is quantum tomography, by which one could obtain the density matrix of the system (*28*) from experimental measurements. However, quantum tomography is more time- and resource-consuming as it scales exponentially with the system size (*29*).

Here, we propose a general practical method to classify entanglement for continuous measurement results. We introduce auxiliary functions to simplify the complicated measurement results and develop a generalized Bell-type inequality for continuous measurements. We also propose an experimental design to test the method in scattering of chemical reactions. Here, we designed a practicable experiment based on the recent scattering experiments of the oriented hydrogen deuteride (HD) and H_2 molecules (*30*). On the basis of the recent experimental data of Zare and co-workers (*30*), we simulate the possible measurement results and demonstrate how to distinguish entangled states from unentangled ones. Moreover, our work also provides the possibility to classify entanglement in other chemical reactions as suggested by Brumer and co-workers for entanglement-assisted coherent control in chemical reactions (*31*, *32*).

BELL'S INEQUALITY FOR CONTINUOUS MEASUREMENT RESULTS

We start by preparing N-particles in a pure state $|\Phi\rangle$. If we perform an r-th measurement on them, then they will collapse on the eigenstate set $\{|\phi_r^1\rangle, |\phi_r^2\rangle, \cdots, |\phi_r^n\rangle\}$. Then, we could expand $|\Phi\rangle$ as

$$|\Phi\rangle = \sum_{i=1}^{n} \alpha_r^i |\phi_r^i\rangle \tag{1}$$

where $|\phi_r^i\rangle$ is the i-th eigenstate corresponding to the measurement r, and $|\Phi\rangle$ is normalized, $\sum_i^n |\alpha_r^i|^2 = 1$. Performing measurement r, we can obtain the measurement results (denoted here by spectrum) $S(|\Phi\rangle\langle\Phi|, r, x)$, where $(|\Phi\rangle\langle\Phi|$ is the density matrix, r represents the measurement r, and the variable x could be, for instance, the scattering angle in the scattering experiment.

The distribution of the measurement results (spectrum) can be written as

$$S(|\Phi\rangle\langle\Phi|, r, x) = \sum_{i}^{n} |\alpha_r^i|^2 \cdot S\left(|\phi_r^i\rangle\langle\phi_r^i|, r, x\right) \tag{2}$$

where $S\left(|\phi_r^i\rangle\langle\phi_r^i|, r, x\right)$ is the spectrum of the state $|\phi_r^i\rangle$ under the r-th measurement.

In the case of the spin system to be discussed in the Supplementary Materials, a quite common example satisfying Eq. 2 is the measurement in the Stern-Gerlach (SG) experiment (*33*) of spin $\frac{1}{2}$ particles. If the particles are prepared in the pure state, then

$$|\Phi\rangle = \alpha_z^+ |\uparrow\rangle + \alpha_z^- |\downarrow\rangle$$

Department of Chemistry, Department of Physics and Astronomy, and Birck Nanotechnology Center, Purdue University, West Lafayette, IN 47907, USA.
*Corresponding author. Email: kais@purdue.edu

Then, providing enough particles to go through that apparatus, the final spectrum can be written as

$$S(|\Phi\rangle\langle\Phi|, r, x) = |\alpha_z^+|^2 \cdot S(|\uparrow\rangle\langle\uparrow|, z, x) + |\alpha_z^-|^2 \cdot S(|\downarrow\rangle\langle\downarrow|, z, x)$$

Here, z represents the direction of the magnetic field in the SG apparatus, and $S(|\uparrow\rangle\langle\uparrow|, z, x)$ and $S(|\downarrow\rangle\langle\downarrow|, z, x)$ describe the distribution of particles detected at different locations, x, on the screen for particles at states $|\uparrow\rangle$ and $|\downarrow\rangle$, respectively.

If these particles are prepared as a mixed state whose density matrix is given by

$$\rho_1 = \sum_{i=1}^{m} p_i |\Phi_i\rangle\langle\Phi_i| \tag{3}$$

where $\sum_{i=1}^{m} p_i = 1$. The spectrum under the r-th measurement is given by

$$S(\rho_1, r, x) = \sum_{i=1}^{m} p_i S(|\Phi_i\rangle\langle\Phi_i|, r, x) \tag{4}$$

In the following section, we will assume that Eqs. 2 and 4 are always satisfied, and we will mainly focus on two-particle systems. Generally, if we use $|\Psi\rangle$ to represent a pure state of the two-particle system, then its density matrix can be written as

$$\rho = \sum_{i=1}^{m} p_i |\Psi_i\rangle\langle\Psi_i| \tag{5}$$

with

$$|\Psi_i\rangle = \sum_{j_1 j_2} c_i(k_1, k_2, j_1, j_2) |\phi_{k_1}^{j_1} \phi_{k_2}^{j_2}\rangle \tag{6}$$

where $\sum_{i=1}^{m} p_i = 1$ and $\sum_{j_1, j_2} |c_i(k_1, k_2, j_1, j_2)|^2 = 1$. Here, $|\phi_{k_1}^{j_1}\rangle$ is the j_1-th eigenstate of a single particle under the k_1-th measurement, and $|\Psi\rangle$ is expanded in the basis set $\{|\phi_{k_1}^{j_1} \phi_{k_2}^{j_2}\rangle\}$. In this section, for simplicity, we only consider the situation that a single particle has just two eigenstates $|\phi_r^+\rangle$ and $|\phi_r^-\rangle$ under the r-th measurement. Positive partial transpose criterion (or the Peres-Horodecki criterion) (*34*) offers us a method to measure entanglement in such a two-particle system: If the partial transpose of the density matrix ρ^{T_B} has any non-negative eigenvalue, then ρ is entangled (*34*, *35*).

Now, we can rewrite Eq. 6 as

$$|\Psi_i\rangle = c_i(r, t, ++)|\phi_r^+ \phi_t^+\rangle + c_i(r, t, +-)|\phi_r^+ \phi_t^-\rangle + c_i(r, t, -+)|\phi_r^- \phi_t^+\rangle + c_i(r, t, --)|\phi_r^- \phi_t^-\rangle \tag{7}$$

Suppose that these particles are divided into two channels, and the r-th and t-th measurements are carried on for channels I and II, respectively, one can obtain the spectrum based on Eq. 2 as

$$\begin{aligned} S(\rho, r, t, x_1, x_2) = &\sum_{i=1}^{m} p_i |c_i(r, t, ++)|^2 \cdot S(|\phi_r^+\rangle\langle\phi_r^+|, r, x_1) S(|\phi_t^+\rangle\langle\phi_t^+|, t, x_2) + \\ &\sum_{i=1}^{m} p_i |c_i(r, t, +-)|^2 \cdot S(|\phi_r^+\rangle\langle\phi_r^+|, r, x_1) S(|\phi_t^-\rangle\langle\phi_t^-|, t, x_2) + \\ &\sum_{i=1}^{m} p_i |c_i(r, t, -+)|^2 \cdot S(|\phi_r^-\rangle\langle\phi_r^-|, r, x_1) S(|\phi_t^+\rangle\langle\phi_t^+|, t, x_2) + \\ &\sum_{i=1}^{m} p_i |c_i(r, t, --)|^2 \cdot S(|\phi_r^-\rangle\langle\phi_r^-|, r, x_1) S(|\phi_t^-\rangle\langle\phi_t^-|, t, x_2) \end{aligned} \tag{8}$$

In the standard Bell's inequality, the experimentally measured correlation is defined as

$$E(r, t) = \frac{N(+,+) + N(-,-) - N(+,-) - N(-,+)}{N(+,+) + N(-,-) + N(+,-) + N(-,+)} \tag{9}$$

where $N(+,+)$ represents number of measurements yielding "+" in both measurement r and measurement t of channels I and II.

These measurement results are used to form the well-known Clauser-Horne-Shimony-Holt (CHSH) inequality (*36*)

$$|E(r, t) + E(r, s) + E(q, s) - E(q, t)| \leq 2 \tag{10}$$

For continuous measurement results, we construct an auxiliary function $V(r, t, x_1, x_2)$ to simplify calculating the correlation function $E(r, t)$. The functional form of the auxiliary function can be found in the Supplementary Materials. The generalized standard Bell's inequality for continuous variables takes the following form

$$\begin{aligned} E = \Big| &\int S(\rho, r, t, x_1, x_2) V(r, t, x_1, x_2) dx_1 dx_2 + \\ &\int S(\rho, q, t, x_1, x_2) V(q, t, x_1, x_2) dx_1 dx_2 + \\ &\int S(\rho, r, s, x_1, x_2) V(r, s, x_1, x_2) dx_1 dx_2 - \\ &\int S(\rho, q, s, x_1, x_2) V(q, s, x_1, x_2) dx_1 dx_2 \Big| \leq 2 \end{aligned} \tag{11}$$

If this inequality (Eq. 11) is violated, then the system is entangled.

EXPERIMENT DESIGN

Recently, Zare and co-workers (*30*) reported the rotationally inelastic collisions between HD and H_2, D_2 molecules at very low temperature. In their scattering experiments, the $|H\rangle$ (orientation of molecules is parallel to their propagating direction) and $|V\rangle$ states (orientation of molecules is vertical to their propagating direction) lead to very different scattering results, which offers us here a possible setup to classify entanglement between molecules based on the scattering results. In this section, we will propose an experimental setting to classify entanglement with continuous measurement results.

In the following simulations, we consider four measurements with respect to four different sets of eigenstate basis. The first one is the scattering measurements corresponding to eigenstates $|H\rangle$ and $|V\rangle$, which we note as measurement Z. The second one corresponds to the eigenstates $|+\rangle = \frac{1}{2}(|H\rangle + |V\rangle)$ and $|-\rangle = \frac{1}{2}(|H\rangle - |V\rangle)$, which we note as measurement X. The other two measurements are taken with the $\frac{Z+X}{\sqrt{2}}$ and $\frac{Z-X}{\sqrt{2}}$ bases.

Measurement results in the Z basis could be taken from the experimental results of Zare and co-workers (*30*), which are continuous as a function of the scattering angles. We assume that the measurements in the X basis and $\frac{Z-X}{\sqrt{2}}$ are projection measurements, so that their results Γ are discrete, which is very common in the experimental setup. To check the derived inequality (Eq. 11), we assume that there is another scattering experiment for measurement $\frac{Z+X}{\sqrt{2}}$, whose results satisfy the Gaussian distribution. In Fig. 1, we show the ideal results (scattering angle θ) of measurement Z (upper part) and $\frac{Z+X}{\sqrt{2}}$ (lower part).

For our simulations, we start by preparing the oriented HD molecules $|v = 1, j = 2, m = 0\rangle$ in state $|H\rangle$, whose orientation is parallel to its

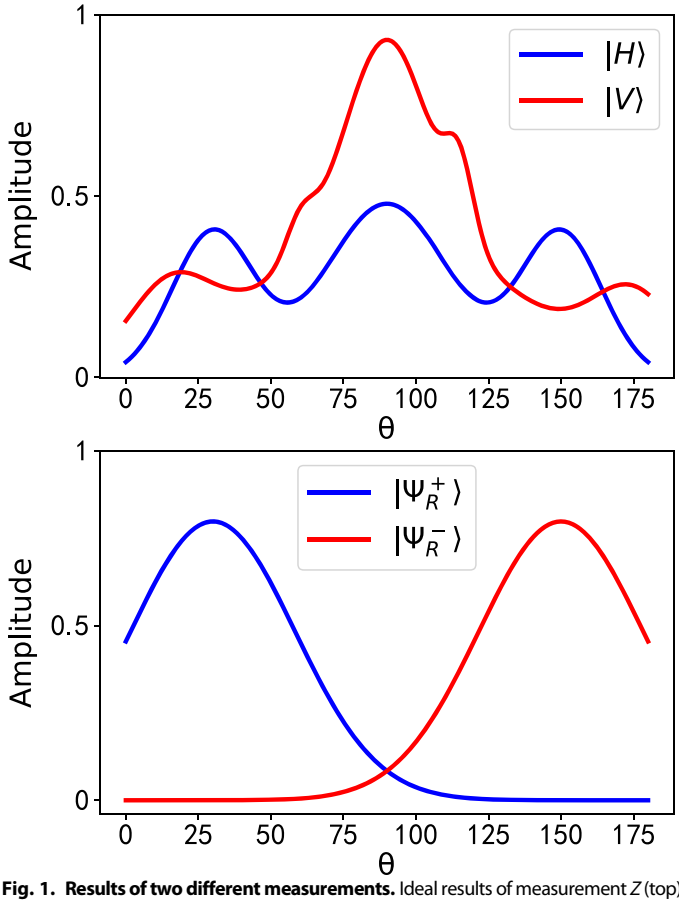

Fig. 1. Results of two different measurements. Ideal results of measurement Z (top) and measurement $\frac{Z+X}{\sqrt{2}}$ (bottom). The results of measurement Z (top) are calculated from (*30*) (Fig. 4, A and B). The blue line $f_H(\theta)$ represents the scattering angle distribution of particles at state $|H\rangle$, and the red line $f_V(\theta)$ represents the scattering angle distribution of particles at state $|V\rangle$. For measurement $\frac{Z+X}{\sqrt{2}}$, its two eigenstates are $|\Psi_R^+\rangle$ and $|\Psi_R^-\rangle$. We assume that the scattering angle distribution $f_\pm(\theta)$ of $|\Psi_R^+\rangle$ and $|\Psi_R^-\rangle$ satisfy the Gaussian distribution. $f_+(\theta) \propto \exp[-(\theta-30)^2/40^2]$ (blue line in the bottom figure); $f_-(\theta) \propto \exp[-(\theta-150)^2/40^2]$ (red line in the bottom figure).

propagation direction (y axis in Fig. 2A), and state $|V\rangle$, whose orientation is vertical (z axis in Fig. 2A). One molecule in group I and another in group II are combined together and then prepared at different states (Werner state, superposition state, or mixed state), as shown in Fig. 2B. For each pair, HD molecules are divided for two channels. In channel I, they will scatter with H_2 clusters. If HD collides with H_2, then the orange sensors will measure the scattering particles, and the scattering results will be performed by measurement Z. If the HD does not collide with H_2 molecules, then the gray sensor will carry on an X measurement (Fig. 2C). In channel II, the scattering process will go through measurement $\frac{Z+X}{\sqrt{2}}$, and HD that are not scattered are measured by $\frac{Z-X}{\sqrt{2}}$.

SIMULATION RESULTS

To perform the simulations, we are going to assume that one can prepare the states from the two oriented molecular beams into the combinations $|H\rangle\,|H\rangle$; $|V\rangle\,|V\rangle$ and $|+\rangle\,|+\rangle$, $|-\rangle\,|-\rangle$ and, finally, the Werner state

$$\rho_w(p) = \frac{p}{2}(\,|HV\rangle + |VH\rangle\,)(\,\langle HV| + \langle VH|\,) + \frac{1-p}{4}I \qquad (12)$$

The free parameter p describes entanglement of the Werner state. $p = 0$ indicates separability, entanglement for $p \le 1/3$, and Bell states of maximum entanglement at $p = 1$ (*37*).

If enough HD molecule pairs are prepared as mentioned above, then the predicted spectra for different initial states are shown in Fig. 3. The simulation is based on data of scattering experiment between HD and H_2 clusters taken from (*30*) (scattering spectrum; Fig. 4, A and B).

We can calculate the density matrix ρ_w for different measurements. For example, if both particles in channels I and II are scattered, then the measurement in the bases $|H\rangle$ and $|V\rangle$ gives

$$\rho_w = \begin{array}{c} \\ |HH\rangle \\ |HV\rangle \\ |VH\rangle \\ |VV\rangle \end{array} \begin{array}{c} \begin{array}{cccc} |HH\rangle & |HV\rangle & |VH\rangle & |VV\rangle \end{array} \\ \begin{pmatrix} \frac{1-p}{4} & 0 & 0 & 0 \\ 0 & \frac{1+p}{4} & \frac{p}{2} & 0 \\ 0 & \frac{p}{2} & \frac{1+p}{4} & 0 \\ 0 & 0 & 0 & \frac{1-p}{4} \end{pmatrix} \end{array} \qquad (13)$$

If we change the basis set, then the density matrix in the bases $|+\rangle$ and $|-\rangle$ gives

$$\rho_w = \begin{array}{c} \\ |++\rangle \\ |+-\rangle \\ |-+\rangle \\ |--\rangle \end{array} \begin{array}{c} \begin{array}{cccc} |++\rangle & |+-\rangle & |-+\rangle & |--\rangle \end{array} \\ \begin{pmatrix} \frac{1+p}{4} & 0 & 0 & -\frac{p}{2} \\ 0 & \frac{1-p}{4} & 0 & 0 \\ 0 & 0 & \frac{1-p}{4} & 0 \\ -\frac{p}{2} & 0 & 0 & \frac{1+p}{4} \end{pmatrix} \end{array} \qquad (14)$$

We could do the same expansion for different measurements. On the basis of Eq. 8, we can predict the results of different initial states, as shown in Fig. 3. The first column represents the simulation results when molecules in both channels are scattered. The second column represents simulation results when HD that goes through channel I is scattered, but not for channel II. The third column represents simulation results when HD that goes through channel II is scattered, but not for channel I. The last column represents results when particles are not scattered.

The state $|HH\rangle$ can be easily classified as its special spectrum in the first column (Ch I, scattered; Ch II, scattered), and state $|++\rangle$ shows significant difference with others in the second (Ch I, scattered; Ch II, not scattered) and third columns (Ch I, not scattered; Ch II, scattered). For the Werner state, they share the same spectrum in the second and third columns, yet their spectrum in the last column (Ch I, not scattered; Ch II, not scattered) offers us some features: Counts for $S_+^1 S_+^2$ and $S_-^1 S_-^2$ will decrease as p increases. Also, the difference in the first column, where there is a subpeak (around $\theta_1 = 30$, $\theta_2 = 90$), increases when p increases. On the basis of these features, it is possible to distinguish them from each other. However, if the initial state is a complex mixed state, then it is impossible for us to derive the initial state because there are infinite possible results of $\sum_{i=1}^m p_i\,|\,c_i(r,t,\pm\pm)\,|^2$ only with restriction $\sum_{i=1}^m p_i = 1$ and $\sum_{j_{1,2}} = \pm\,|\,c_i(r,t,j_1,j_2)\,|^2 = 1$. However, with more information of p_i, there is a chance to resolve the quantum state. For example, if we have already known that the pairs are at the Werner state, then we could obtain the quantum state, as shown in the simulation work.

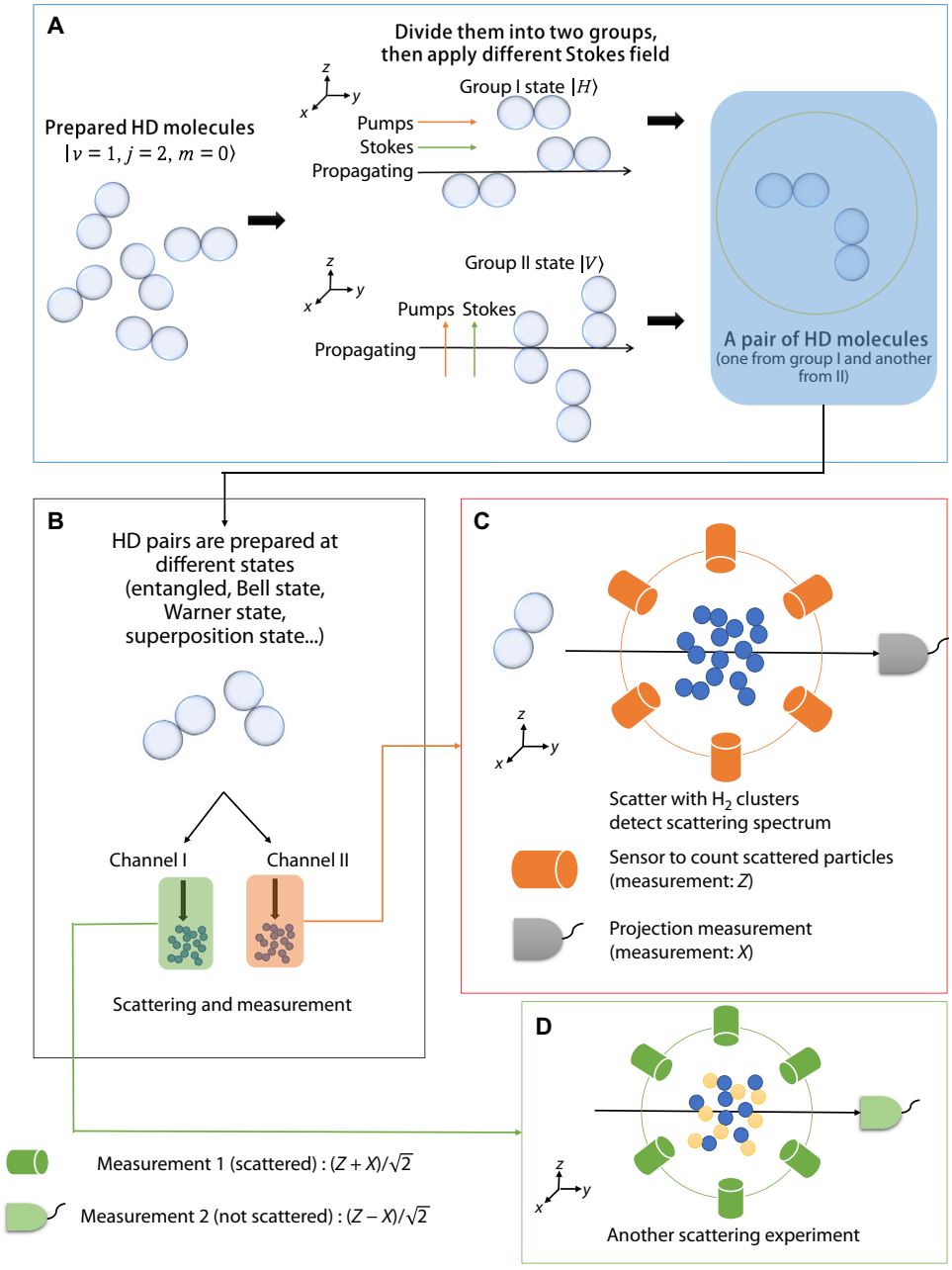

Fig. 2. Sketch of the experiment design. (**A**) HD molecules are prepared in the state $|v = 1, j = 2, m = 0\rangle$ using Stark-induced adiabatic Raman passage (SARP) (*30*). Then, we can divide them into two molecular beams (two groups). If we apply the Pumps and Stokes electric field along the *y* axis, then HD in group I is set at state $|H\rangle$ (orientation of HD is along the *y* axis, parallel to the direction of its propagation). The molecule HD in group II is set at state $|V\rangle$ (orientation of HD is along the *z* axis, norm to the direction of its propagation). One molecule from group I and another from group II are combined together, and then, HD pairs are prepared at different initial states (if we do nothing, then these pairs will stay on a mixed state $|H\rangle \otimes |V\rangle$). (**B**) The specific prepared state will go through two channels, molecule in channel I will scatter with H_2 clusters, where the bond axis of H_2 is distributed isotropically. (**C**) Sensors (orange) are used to detect scattered particles and count numbers for each angle (*Z* measurement). Molecules that are not scattered will go to another sensor (gray), by which they will be measured on the eigenstates $|+\rangle$ and $|-\rangle$ (*X* measurement). (**D**) In channel II, we set another experiment, so that scattered prepared HD molecules with isotropically distributed H_2 clusters are measured under $\frac{Z+X}{\sqrt{2}}$, while the others are measured under $\frac{Z-X}{\sqrt{2}}$.

MATERIALS AND METHODS

Here, we show how to obtain the simulation results. As an example, we will take the first row in Fig. 3 (state $|HH\rangle$: channel I, scattered; channel II, scattered). Consider the HD molecule that goes through channel I. If the molecule HD scatted with a probability P_{scatter}, then the random number generator (RNG), where we assume that the RNG produces random numbers with uniform distribution, produces a number a_1, $0 \le a_1 \le 1$. If $a_1 \le P_{\text{scatter}}$, then this HD molecule with a specific state will collide with H_2 clusters; otherwise, it will be measured by the gray sensor as shown in Fig. 2. For the scattered HD molecules,

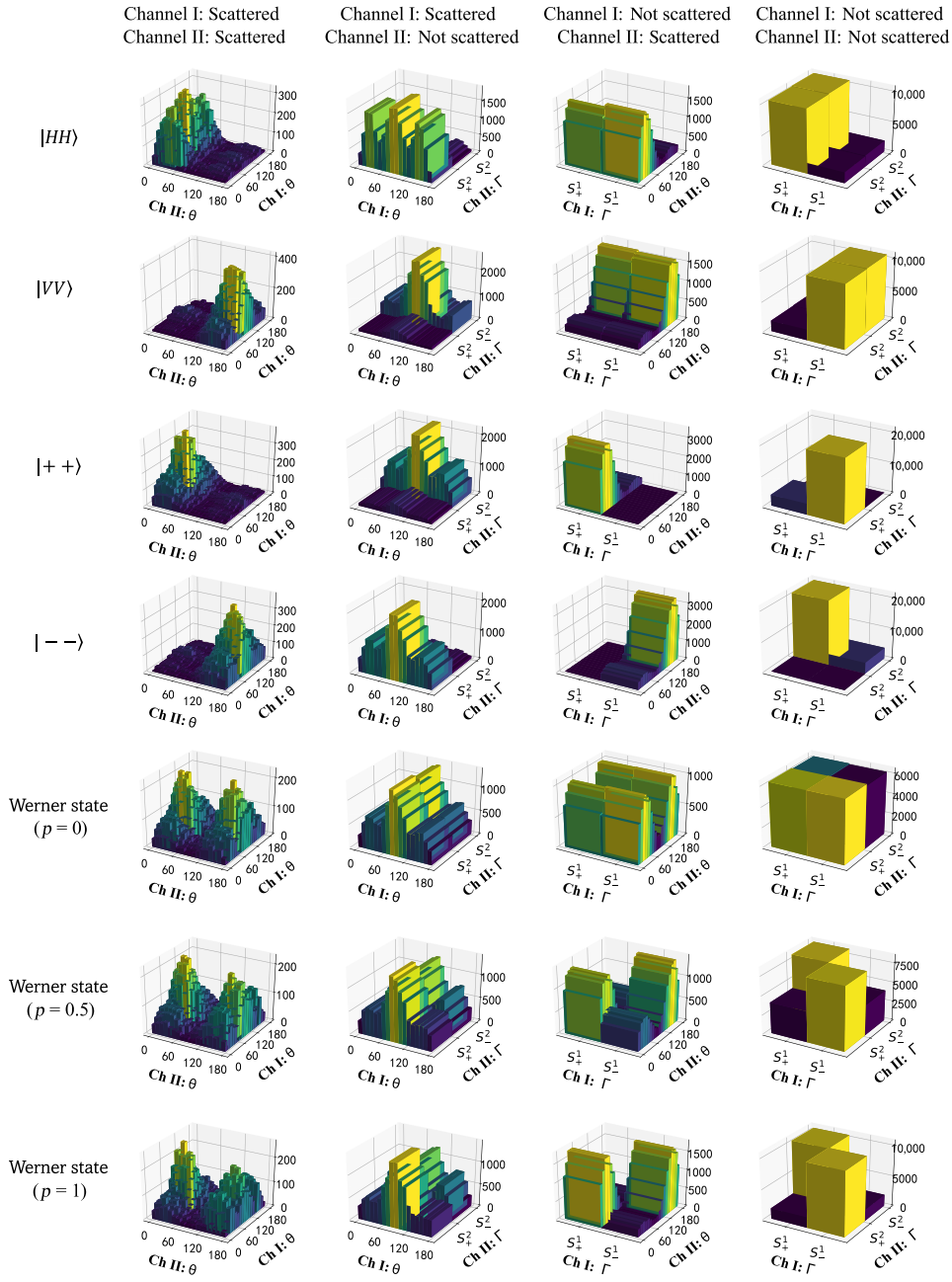

Fig. 3. Simulation results of the scattering experiments. The figure shows histograms of the simulation count results (*z* axis in the figure) as a function of different measures in channel I and channel II. Row 1: The spectrum for the separable state $|HH\rangle$, both HD molecules are in the state $|H\rangle$. Row 2: The spectrum for separable state $|VV\rangle$. Row 3: The spectrum for the superposition state $|++\rangle$, where $|+\rangle = \frac{1}{\sqrt{2}}(|H\rangle + |D\rangle)$. Row 4: The spectrum for the superposition state $|--\rangle$, where $|-\rangle = \frac{1}{\sqrt{2}}(|H\rangle - |D\rangle)$. Rows 5, 6, and 7: The spectrum for the Werner state $\rho_w(p)$. When $p = 1$, the prepared pairs are at the Bell state $\frac{1}{\sqrt{2}}(|HD\rangle + |DH\rangle)$.

the scattering spectrum (measurement distribution) is $f_H(\theta)$, as shown in Fig. 1, where θ represents scattering angles, and we can get $f_H(\theta)$ by fitting the results in the experimental measurements of Zare and co-workers (*30*). If the HD molecule at state $|H\rangle$ is scattered, then the following process is used to generate its scattering angle: A random angle $0 \le \theta \le 180$ and a random number a_2, $0 \le a_2 \le 1$ are produced by RNG. If $a_2 \le f_H(\theta)$, then we accept θ as the scattering angle; otherwise, this process is repeated. For the molecules that are not scattered, as $|H\rangle = \frac{1}{\sqrt{2}}(|+\rangle + |-\rangle)$, the measurement result has half possibility to be S_+ and another half to be S_-. We can use one random number to simulate the measurement results of these unscattered molecules.

DISCUSSION AND CONCLUSION

In the measurement setting of the Werner state, Eq. 11 is violated when $p > \frac{1}{\sqrt{2}}$. Meanwhile, we know that the Werner state will be an entangled state when $p > \frac{1}{3}$. Hence, violation of Eq. 11 guarantees existence of entanglement, yet the nonviolation of the inequality does not exclude the possibility of entanglement.

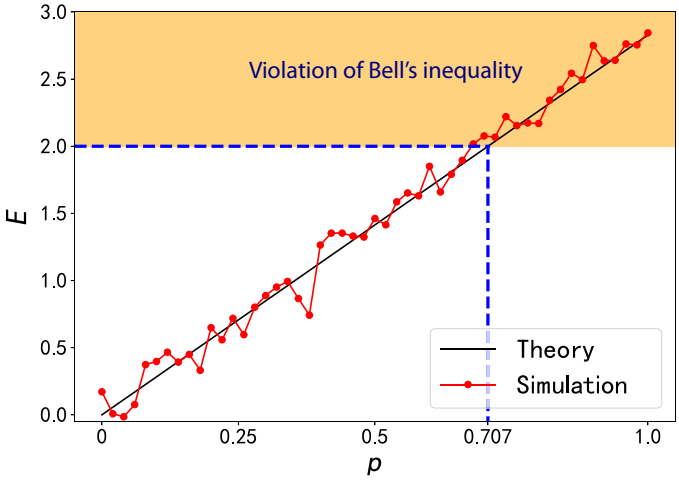

Fig. 4. Theory and simulation results for *E* of particle pairs at different Werner state $\rho_w(p)$. To calculate the integral, we divided scattering angles into 18 slots (10° per slot). We studied 1×10^6 particles in simulation, and possibility to be scattered is set as 0.4.

As shown in Fig. 4, the simulation result (red) E is very close to the theory result (black). The difference is mostly due to the statistical error (please refer to the Supplementary Materials for method in simulation). We studied 1×10^6 particles and divided scattering angles into 18 slots uniformly. We also want to mention that, if we divide the scattering angle into too many or too few slots ($\leq$10 or $\geq$50), then the simulation result E will be much further from the theory prediction.

In summary, we have generalized the standard Bell's inequality from discrete to continuous measurement results. We designed an experiment setting as a potential application of violating the Bell's inequality. We performed theoretical simulations to show the validity of the proposed experiment. The method is general and might be used to design and classify entanglement in new molecular scattering experiments.

SUPPLEMENTARY MATERIALS

Supplementary material for this article is available at http://advances.sciencemag.org/cgi/content/full/5/8/eaax5283/DC1

Section SA. Bell's inequality for continuous measurement results
Section SB. Details of the simulation method
Section SC. An example of spin $\frac{1}{2}$ particles
Fig. S1. Sketch of Bell's experiment of spin $\frac{1}{2}$ particles.
Fig. S2. Simulation result (1z2z).
Fig. S3. Simulation result (1z2x).
Fig. S4. Simulation result (1x2z).
Fig. S5. Simulation result (1x2x).
Fig. S6. Simulation result (Werner state, $\rho = 0.6$).
References (*38*–*40*)

REFERENCES AND NOTES

1. E. Schrödinger, Die gegenwärtige situation in der quantenmechanik. *Naturwissenschaften* **23**, 823–828 (1935).
2. A. Einstein, B. Podolsky, N. Rosen, Can quantum-mechanical description of physical reality be considered complete? *Phys. Rev.* **47**, 777 (1935).
3. J. S. Bell, On the Einstein Podolsky Rosen paradox. *Physics. Physique. Fizika.* **1**, 195 (1964).
4. A. Aspect, P. Grangier, G. Roger, Experimental tests of realistic local theories via Bell's theorem. *Phys. Rev. Lett.* **47**, 460 (1981).
5. R. Ursin, F. Tiefenbacher, T. Schmitt-Manderbach, H. Weier, T. Scheidl, M. Lindenthal, B. Blauensteiner, T. Jennewein, J. Perdigues, P. Trojek, B. Ömer, M. Fürst, M. Meyenburg, J. Rarity, Z. Sodnik, C. Barbieri, H. Weinfurter, A. Zeilinger, Entanglement-based quantum communication over 144 km. *Nat. Phys.* **3**, 481–486 (2007).
6. W. Zhang, D.-S. Ding, Y.-B. Sheng, L. Zhou, B.-S. Shi, G.-C. Guo, Quantum secure direct communication with quantum memory. *Phys. Rev. Lett.* **118**, 220501 (2017).
7. F. Mazeas, M. Traetta, M. Bentivegna, F. Kaiser, D. Aktas, W. Zhang, C. A. Ramos, L. A. Ngah, T. Lunghi, É. Picholle, N. Belabas-Plougonven, X. Le Roux, É. Cassan, D. Marris-Morini, L. Vivien, G. Sauder, L. Labonté, S. Tanzilli, High-quality photonic entanglement for wavelength-multiplexed quantum communication based on a silicon chip. *Opt. Express* **24**, 28731–28738 (2016).
8. P. Kurpiers, P. Magnard, T. Walter, B. Royer, M. Pechal, J. Heinsoo, Y. Salathé, A. Akin, S. Storz, J.-C. Besse, S. Gasparinetti, A. Blais, A. Wallraff, Deterministic quantum state transfer and remote entanglement using microwave photons. *Nature* **558**, 264–267 (2018).
9. A. Sørensen, K. Mølmer, Entanglement and quantum computation with ions in thermal motion. *Phys. Rev. A* **62**, 022311 (2000).
10. Y.-B. Sheng, L. Zhou, Deterministic entanglement distillation for secure double-server blind quantum computation. *Sci. Rep.* **5**, 7815 (2015).
11. J. L. O'Brien, Optical quantum computing. *Science* **318**, 1567–1570 (2007).
12. R. Jozsa, N. Linden, On the role of entanglement in quantum-computational speed-up, in *Proceedings of the Royal Society of London A: Mathematical, Physical and Engineering Sciences* (The Royal Society, 2003), vol. 459, pp. 2011–2032.
13. A. Ekert, R. Jozsa, P. Marcer, Quantum algorithms: Entanglement-enhanced information processing. *Philos. Trans. R. Soc. Lond. Ser. A Math. Phys. Eng. Sci.* **356**, 1769–1782 (1998).
14. Q. Wei, Y. Cao, S. Kais, B. Friedrich, D. Herschbach, Quantum computation using arrays of *N* polar molecules in pendular states. *Chemphyschem* **17**, 3714–3722 (2016).
15. S. Kais, Entanglement, electron correlation, and density matrices. *Adv. Chem. Phys.* **134**, 493 (2007).
16. C. Reimer, M. Kues, P. Roztocki, B. Wetzel, F. Grazioso, B. E. Little, S. T. Chu, T. Johnston, Y. Bromberg, L. Caspani, D. J. Moss, R. Morandotti, Generation of multiphoton entangled quantum states by means of integrated frequency combs. *Science* **351**, 1176–1180 (2016).
17. X.-L. Wang, L.-K. Chen, W. Li, H.-L. Huang, C. Liu, C. Chen, Y.-H. Luo, Z.-E. Su, D. Wu, Z.-D. Li, H. Lu, Y. Hu, X. Jiang, C.-Z. Peng, L. Li, N.-L. Liu, Y.-A. Chen, C.-Y. Lu, J.-W. Pan, Experimental ten-photon entanglement. *Phys. Rev. Lett.* **117**, 210502 (2016).
18. M. Bayer, P. Hawrylak, K. Hinzer, S. Fafard, M. Korkusinski, Z. R. Wasilewski, O. Stern, A. Forchel, Coupling and entangling of quantum states in quantum dot molecules. *Science* **291**, 451–453 (2001).
19. P. Neumann, N. Mizuochi, F. Rempp, P. Hemmer, H. Watanabe, S. Yamasaki, V. Jacques, T. Gaebel, F. Jelezko, J. Wrachtrup, Multipartite entanglement among single spins in diamond. *Science* **320**, 1326–1329 (2008).
20. K. Mølmer, A. Sørensen, Multiparticle entanglement of hot trapped ions. *Phys. Rev. Lett.* **82**, 1835 (1999).
21. W. B. Gao, P. Fallahi, E. Togan, J. Miguel-Sánchez, A. Imamoglu, Observation of entanglement between a quantum dot spin and a single photon. *Nature* **491**, 426–430 (2012).
22. G. Tóth, O. Gühne, Detecting genuine multipartite entanglement with two local measurements. *Phys. Rev. Lett.* **94**, 060501 (2005).
23. N. J. Cerf, C. Adami, Entropic Bell inequalities. *Phys. Rev. A* **55**, 3371 (1997).
24. J. Gao, L.-F. Qiao, Z.-Q. Jiao, Y.-C. Ma, C.-Q. Hu, R.-J. Ren, A.-L. Yang, H. Tang, M.-H. Yung, X.-M. Jin, Experimental machine learning of quantum states. *Phys. Rev. Lett.* **120**, 240501 (2018).
25. J. Wenger, M. Hafezi, F. Grosshans, R. Tualle-Brouri, P. Grangier, Maximal violation of bell inequalities using continuous-variable measurements. *Phys. Rev. A* **67**, 012105 (2003).
26. Z.-B. Chen, J.-W. Pan, G. Hou, Y.-D. Zhang, Maximal violation of Bell's inequalities for continuous variable systems. *Phys. Rev. Lett.* **88**, 040406 (2002).
27. Q. Y. He, E. G. Cavalcanti, M. D. Reid, P. D. Drummond, Bell inequalities for continuous-variable measurements. *Phys. Rev. A* **81**, 062106 (2010).
28. G. M. D'Ariano, P. Lo Presti, Quantum tomography for measuring experimentally the matrix elements of an arbitrary quantum operation. *Phys. Rev. Lett.* **86**, 4195 (2001).
29. J. B. Altepeter, D. F. V. James, P. G. Kwiat, 4 qubit quantum state tomography, in *Quantum State Estimation* (Springer, 2004), pp. 113–145.
30. W. E. Perreault, N. Mukherjee, R. N. Zare, Cold quantum-controlled rotationally inelastic scattering of HD with H_2 and D_2 reveals collisional partner reorientation. *Nat. Chem.* **10**, 561–567 (2018).
31. V. Zeman, M. Shapiro, P. Brumer, Coherent control of resonance-mediated reactions: F + HD. *Phys. Rev. Lett.* **92**, 133204 (2004).
32. J. Gong, M. Shapiro, P. Brumer, Entanglement-assisted coherent control in nonreactive diatom–diatom scattering. *J. Chem. Phys.* **118**, 2626–2636 (2003).
33. W. Gerlach, O. Stern, Der experimentelle nachweis der richtungsquantelung im magnetfeld. *Z Phys.* **9**, 349–352 (1922).
34. A. Peres, Separability criterion for density matrices. *Phys. Rev. Lett.* **77**, 1413 (1996).

35. O. Rudolph, Computable cross-norm criterion for separability. *Lett. Math. Phys.* **70**, 57–64 (2004).
36. J. F. Clauser, M. A. Horne, A. Shimony, R. A. Holt, Proposed experiment to test local hidden-variable theories. *Phys. Rev. Lett.* **23**, 880 (1969).
37. R. F. Werner, Quantum states with Einstein-Podolsky-Rosen correlations admitting a hidden-variable model. *Phys. Rev. A* **40**, 4277 (1989).
38. M. Horodecki, P. Horodecki, R. Horodecki, Separability of *n*-particle mixed states: Necessary and sufficient conditions in terms of linear maps. *Phys. Lett. A* **283**, 1–7 (2001).
39. J. Lee, M. S. Kim, Entanglement teleportation via werner states. *Phys. Rev. Lett.* **84**, 4236 (2000).
40. Y. Yeo, Teleportation via thermally entangled states of a two-qubit heisenberg *XX* chain. *Phys. Rev. A* **66**, 062312 (2002).

Acknowledgments: The authors thank A. Hu, R. Xia, and T. Bian for the useful discussions. **Funding:** This study is based on work supported by the U.S. Department of Energy, Office of Basic Energy Sciences, under award number DE-SC0019215. **Author contributions:** S.K. developed and supervised the project. J.L. performed the calculations. Both authors performed the data analysis and modeling and contributed to the writing of the manuscript. **Competing interests:** The authors declare that they have no competing interests. **Data and materials availability:** All data needed to evaluate the conclusions in the paper are present in the paper and/or the Supplementary Materials. Additional data related to this paper may be requested from the authors.

Submitted 31 March 2019
Accepted 24 June 2019
Published 2 August 2019
10.1126/sciadv.aax5283

Citation: J. Li, S. Kais, Entanglement classifier in chemical reactions. *Sci. Adv.* **5**, eaax5283 (2019).